

Article

Study of Dependence of Kinetic Freezeout Temperature on the Production Cross-Section of Particles in Various Centrality Intervals in Au–Au and Pb–Pb Collisions at High Energies

Muhammad Waqas ¹  and Guang-Xiong Peng ^{2,*}

¹ School of Nuclear Science and Technology, University of Chinese Academy of Sciences, Beijing 100049, China; waqas_phy313@yahoo.com or waqas_phy313@ucas.ac.cn

² Theoretical Physics Center for Science Facilities, Institute of High Energy Physics, Beijing 100049, China

* Correspondence: gxpeng@ucas.ac.cn

Abstract: Transverse momentum spectra of π^+ , p , Λ , Ξ or Ξ^+ , Ω or Ω^+ and deuteron (d) in different centrality intervals in nucleus–nucleus collisions at the center of mass energy are analyzed by the blast wave model with Boltzmann Gibbs statistics. We extracted the kinetic freezeout temperature, transverse flow velocity and kinetic freezeout volume from the transverse momentum spectra of the particles. It is observed that the non-strange and strange (multi-strange) particles freezeout separately due to different reaction cross-sections. While the freezeout volume and transverse flow velocity are mass dependent, they decrease with the resting mass of the particles. The present work reveals the scenario of a double kinetic freezeout in nucleus–nucleus collisions. Furthermore, the kinetic freezeout temperature and freezeout volume are larger in central collisions than peripheral collisions. However, the transverse flow velocity remains almost unchanged from central to peripheral collisions.

Keywords: non-strange; strange; multi-strange; kinetic freeze-out temperature; transverse flow velocity; freezeout volume; cross-section; centrality bins; transverse momentum spectra

PACS: 12.40.Ee; 13.85.Hd; 25.75.Ag; 25.75.Dw; 24.10.Pa



Citation: Waqas, M.; Peng, G.-X. Study of Dependence of Kinetic Freezeout Temperature on the Production Cross-Section of Particles in Various Centrality Intervals in Au–Au and Pb–Pb Collisions at High Energies. *Entropy* **2021**, *23*, 488. <https://doi.org/10.3390/e23040488>

Academic Editor: Lawrence Horwitz

Received: 21 March 2021

Accepted: 12 April 2021

Published: 20 April 2021

Publisher's Note: MDPI stays neutral with regard to jurisdictional claims in published maps and institutional affiliations.



Copyright: © 2021 by the authors. Licensee MDPI, Basel, Switzerland. This article is an open access article distributed under the terms and conditions of the Creative Commons Attribution (CC BY) license (<https://creativecommons.org/licenses/by/4.0/>).

1. Introduction

Freezeout stages are very important because they provide essential information about the emissions of the particles at those stages. Generally, there are two freezeout stages found in the literature—namely, the chemical freezeout and kinetic freezeout stage—and both of these correspond to their respective temperatures. The chemical freezeout is the intermediate stage in high-energy collisions where the intra-nuclear collisions between the particles are inelastic and the ratio of various types of particles remain unchanged; the temperature of the particles at this stage is the chemical freezeout temperature, which describes the excitation degree of the system at the chemical freezeout stage. Correspondingly, the thermal/kinetic freezeout is the last stage in high-energy collisions. At this stage, the intra-nuclear collisions between the particles are elastic. The transverse momentum distributions of various kinds of particles are no longer changed at the thermal freezeout stage, and the temperature at this stage is called the kinetic freezeout temperature.

According to the thermal and statistical model [1–4], the chemical freezeout temperature (T_{ch}) in central nucleus–nucleus collisions increases with the increase of the collision energy from a few GeV to above 10 GeV and then saturates in an energy range of more than 12 GeV. At the Relativistic Heavy Ion Collider (RHIC) and Large Hadron Collider (LHC), the maximum T_{ch} is 160 MeV, although there is a slight decrease from the energy of RHIC to LHC, but the situation of the kinetic freezeout temperature (T_0) is complex. At first, T_0 in central collisions increases with the collision energy increasing from a few GeV to above 10 GeV, but this tendency can either be saturated, decreasing or increasing. On

the other hand, T_{ch} in central nucleus–nucleus collisions is a little larger than in peripheral nucleus–nucleus collisions; however, there are three possible trends of T_0 from central to peripheral collisions, which are (1) T_0 increases from central to peripheral collisions, (2) T_0 decreases from central to peripheral collisions, and (3) T_0 remains constant from central to peripheral collisions. It is very important to search for the correct trend of T_0 with energy and centrality. Furthermore, there are different kinetic freezeout scenarios found in the literature, which include single, double, triple and multiple kinetic freezeout scenarios [5–10]. In the single kinetic freezeout scenario, one set of parameters is used for the strange, multi-strange and non-strange particles. In the double kinetic freezeout scenario, one set of parameters is used for strange (multi-strange) and another for non-strange particles; separate sets of parameters are used for strange, multi-strange and non-strange particles in the triple kinetic freezeout scenario. In contrast, in the multiple kinetic freezeout scenario, separate sets of parameters are used for each particle. The trend of transverse flow velocity (β_T) and freezeout volume (V) with energy is an increasing trend in most of the literature [6,11–16]. Most of the literature claims to show a decreasing (or invariant) trend of β_T and V from central to peripheral collisions [10,15–18].

The transverse momentum spectra (p_T) of the particles are very important observable variables due to the fact that they provide essential information about the equilibrium dynamics and isotropy of the system in high-energy collisions [9]. In the present work, we analyze the p_T spectra of π^+ , p , Λ , Ξ (Ξ^+), Ω (Ω^+) and deuteron (d) in nucleus–nucleus collisions at the center of mass energy.

The remainder of the paper consists of the method and formalism in Section 2 and results and discussion in Section 3, and the summary of our main observations and conclusions are presented in Section 4.

2. Method and Formalism

There are various models suggested for the extraction of T_0 , V and β_T ; e.g., the blast wave model with Boltzmann Gibbs statistics (BGBW) [19–21], the blast wave model with Tsallis statistics (TBW) [22–24], an alternative method by using Tsallis statistics [25–31] and an alternative method by using the blast wave model with Boltzmann Gibbs statistics [32–37]. In this work, we choose the blast wave model with Boltzmann Gibbs statistics, which is a phenomenological model and is used for the spectra of hadrons based on the flow of local thermal sources with global variables of temperature, volume and transverse flow velocity.

According to [38–40], the p_T distribution of the BGBW can be written as

$$f(p_T) = \frac{1}{N} \frac{dN}{dp_T} = C \frac{gV}{(2\pi)^2} p_T m_T \int_0^R r dr \times I_0 \left[\frac{p_T \sinh(\rho_1)}{T_0} \right] K_1 \left[\frac{m_T \cosh(\rho_1)}{T_0} \right], \quad (1)$$

where C stands for the normalization constant, g represents the degeneracy factor of the particles, V is the freezeout volume, $m_T = \sqrt{p_T^2 + m_0^2}$ is the transverse mass (m_0 is the resting mass of the particle), r is the radial coordinate, R is the maximum r , $\rho = \tanh^{-1}[\beta(r)]$ is the boost angle, $\beta(r) = \beta_S(r/R)^{n_0}$ is a self-similar flow profile, and β_S is the flow velocity on the surface, as a mean of $\beta(r)$, $\beta_T = (2/R^2) \int_0^R r \beta(r) dr = 2 \beta_S / (n_0 + 2)$ if $n_0 = 2$, $\beta_T = 0.5 \beta_S$, because the maximum β_S is 1c and the maximum value of β_T is 0.5; however, if $n_0 = 1$, this will result in $\beta_T = (2/3) \beta_S$, and thus the maximum β_T is $(2/3)c$. However, if n_0 is used as a free parameter [41], it increases the value of 854 by several times in terms of the number of free parameters. I_0 and K_1 are the Bessel-modified functions of the first and second kind, respectively.

Equation (1) is not sufficient for the description of all p_T spectra, particularly when the maximum p_T reaches 100 GeV/c for collisions at the LHC [42], where several p_T regions [43] have been observed by the model analysis. These regions include the first p_T region with $p_T < 4.5$ GeV/c, the second and third region with $4\text{--}6$ GeV/c $< p_T <$

17–20 GeV/c and $p_T > 17\text{--}20$ GeV/c, respectively. It is expected that different p_T regions correspond to different interaction mechanisms, such as the effects and changes according to the medium, nuclear transparency and the effect of the number of strings etc., which are discussed in detail in [17]. Therefore, for the complete description of the entire p_T , we can use functions such as Tsallis Levy [44,45] and the Hagedorn function [42,46,47] for the spectra in high and very high p_T regions, and this corresponds to the inverse power law. In this work, we used the inverse power law to describe the p_T spectra in high p_T regions; that is,

$$f_H(p_T) = \frac{1}{N} \frac{dN}{dp_T} = Ap_T \left(1 + \frac{p_T}{p_0} \right)^{-n}, \quad (2)$$

where N and A represents the number of particles and normalization constant, respectively, and p_0 and n are the free parameters. There are several modified versions of the Hagedorn function found in the literature [48–54].

Generally, the two main processes responsible for the contribution of p_T spectra are soft excitation (which contributes the soft component in the low p_T region) and the hard scattering process (which contributes over the whole p_T region). Equation (1) is taken into account for the soft excitation process and Equation (2) for the hard scattering process. Equations (1) and (2) can be superposed by two methods; i.e., (1) the super position principle, where the contribution regions of components overlap each other, and (2) the Hagedorn model (usual step function), when there is no overlapping of different regions of different components. According to the first method,

$$f_0(p_T) = kf_S(p_T) + (1 - k)f_H(p_T), \quad (3)$$

where k represents the contribution fraction of the first component and $(1 - k)$ represents the contribution function of the second component.

The usual step function can be used to structure the superposition of Equations (1) and (2). According to Hagedorn model [42,46,47], the usual step function can also be used for the superposition of the two functions, as

$$f_0(p_T) = A_1\theta(p_1 - p_T)f_1(p_T) + A_2\theta(p_T - p_1)f_2(p_T), \quad (4)$$

where A_1 and A_2 are the fraction constants which give the two components to be equal to each other at $p_T = p_1$.

It should be noted that the soft and hard components in Equations (3) and (4) are treated in different ways over the whole p_T region. Equation (3) is used for the contribution of the soft component in the range 0–2~3 GeV/c or a little more. However, in the case of the contribution of the hard component, even though the main contribution in the low p_T region is the soft excitation process, it covers the whole p_T region. In Equation (4), in the range from 0 to p_1 and from p_1 up to the maximum, the contributions of the soft and hard components are present, respectively, and there is no mixed region for the two components. In addition, we would like to point out that, in the present work, we have used Equation (1) (which is a single-component BGBW) only, but Equations (3) and (4) are stated in order to present the entire methodology and treatment (if Equation (2) is used). If we were to use a double-component BGBW, then we could use either Equations (3) or (4) to combine the two components.

3. Results and Discussion

Figure 1 demonstrates the transverse momentum (p_T) spectra, $[(1/2\pi p_T) d^2N/dydp_T]$ or $[1/N_{ev}(1/2\pi p_T) d^2N/dydp_T]$ of π^+ , p , Λ , Ξ^+ , $\bar{\Omega}^+$ and deuteron (d) in various centrality classes in Au–Au collisions at 62.4 GeV. The spectra are distributed in different centrality classes; e.g., for π^+ and p , 0–5%, 5–10%, 10–20%, 20–30%, 30–40%, 40–50%, 50–60%, 60–70% and 70–80%, for Λ , 0–5%, 5–10%, 10–20%, 20–30%, 30–40%, 40–60% and 60–80%, for Ξ^+ ,

0–5%, 5–10%, 10–20%, 20–40%, 40–60% and 60–80%, for $\bar{\Omega}^+$, 0–20%, 20–40% and 40–60% at $|y| < 0.1$, and for deuteron (d), 0–10%, 10–20%, 20–40%, 40–60% and 60–80%, at $|y| < 0.3$. The symbols are cited from the experimental data measured by the STAR Collaboration at the Relativistic Heavy Ion Collider (RHIC) [21,55,56]. In the figure, the curves are our fitted results from Equation (1). The corresponding values of the free parameters (T_0 , V , β_T and n_0), normalization constant (N_0), χ^2 and number of degrees of freedom (ndof) are listed in Table 1, the parameter trend of which is analyzed and discussed later in this section. One can see that the p_T spectra of the particles are shown to obey approximately the blast wave model with Boltzmann Gibbs statistics. Furthermore, the spectra of π^+ in 5–10%, 10–20%, 20–30%, 30–40%, 40–50%, 50–60%, 60–70% and 70–80% centrality intervals are scaled with 1/3, 1/7, 1/18, 1/40, 1/100, 1/250, 1/700 and 1/1500 respectively, while the centrality intervals 5–10%, 10–20%, 20–30%, 30–40%, 40–50%, 50–60%, 60–70% and 70–80% of p are scaled by 1/3, 1/7, 1/26, 1/60, 1/150, 1/250, 1/400 and 1/600, respectively.

Figure 2 is similar to Figure 1, but it shows the the p_T spectra of π^+ , p , Λ , Ξ , Ω and deuteron (d) in different centrality intervals in Pb–Pb collisions at 2.76 TeV. The spectra are distributed in different centrality intervals; e.g., for π^+ , and p ; 0–5%, 5–10%, 10–20%, 20–30%, 30–40%, 40–50%, 50–60%, 60–70% 70–80% and 80–90% at $|y| < 0.5$, for Λ , Ξ , and Ω ; 0–10%, 10–20%, 20–40%, 40–60% and 60–80%, for Ω ; 0–10%, 10–20%, 20–40%, 40–60% and 60–80% at $y = 0$, and for deuteron (d); 0–10%, 10–20%, 20–40%, 40–60% and 60–80%, at $|y| < 0.5$. The spectra of π^+ and p in 5–10%, 10–20%, 20–30%, 30–40%, 40–50%, 50–60%, 60–70% and 70–80% centrality intervals are scaled with 1/2, 1/4, 1/6, 1/8, 1/10, 1/10, 1/10, 1/10 and 1/10, respectively. The symbols are cited from the experimental data measured by the ALICE Collaboration at the Large Hadron Collider (LHC) [57–59]. In the figure, the curves are our fitted results with a result of 231 (1). The corresponding values of free parameters (T_0 , V , β_T and n_0), normalization constant (N_0), χ^2 and number of degrees of freedom (ndof) are listed in Table 1, the parameter trend of which is analyzed and discussed below. One can see that the p_T spectra of the particles are shown to obey approximately the blast wave model with Boltzmann Gibbs statistics. Note that we have used the method of least squares to obtain the parameters in the present work, and the fits (especially the ALICE data) to the BGBW model are not good for quite abundant hadron species, such as π^+ and protons, due to the generation of non-inclusion resonance in the low p_T region. In addition, we would also like to point out that the values of χ^2 vary, especially in some cases in central collisions, where it increases due to poor fitting.

Table 1. Values of free parameters (T_0 and β_T , V , normalization constant (N_0), n_0), χ^2 and degree of freedom (dof) corresponding to the curves in Figures 1 and 2

Collisions	Centrality	Particle	T_0 (GeV)	β_T (c)	V (fm^3)	N_0	n_0	χ^2/dof
Figure 1 Au–Au 62.4 GeV	0–5%	π^+	0.111 ± 0.005	0.520 ± 0.008	5000 ± 193	0.25 ± 0.06	0.8	3/5
	5–10%	–	0.107 ± 0.004	0.518 ± 0.008	4800 ± 170	0.24 ± 0.004	1.3	7/5
	10–20%	–	0.103 ± 0.005	0.520 ± 0.009	4615 ± 165	0.185 ± 0.004	2.6	2/5
	20–30%	–	0.098 ± 0.006	0.515 ± 0.011	4430 ± 161	0.136 ± 0.0005	1.3	2/5
	30–40%	–	0.095 ± 0.004	0.517 ± 0.009	4250 ± 160	0.0975 ± 0.004	1.2	2/5
	40–50%	–	0.090 ± 0.006	0.512 ± 0.010	4000 ± 150	0.067 ± 0.004	1.8	5/5
	50–60%	–	0.086 ± 0.005	0.514 ± 0.010	3800 ± 150	0.049 ± 0.005	2	7/5
	60–70%	–	0.081 ± 0.005	0.513 ± 0.011	3610 ± 170	0.029 ± 0.004	2	1/5
	70–80%	–	0.080 ± 0.004	0.510 ± 0.007	3400 ± 176	0.015 ± 0.005	2	4/5
Figure 1 Au–Au 62.4 GeV	0–5%	p	0.113 ± 0.006	0.490 ± 0.010	4700 ± 170	0.0165 ± 0.003	1.2	33/9
	5–10%	–	0.109 ± 0.005	0.500 ± 0.011	4530 ± 160	0.0094 ± 0.0005	1	20/9
	10–20%	–	0.105 ± 0.004	0.500 ± 0.009	4400 ± 155	0.0113 ± 0.004	1.2	5/9
	20–30%	–	0.100 ± 0.005	0.490 ± 0.010	4225 ± 140	0.008 ± 0.0005	1.3	3/9
	30–40%	–	0.097 ± 0.005	0.488 ± 0.011	4160 ± 150	0.0055 ± 0.0004	1.5	7/9
	40–50%	–	0.093 ± 0.005	0.489 ± 0.009	3900 ± 150	0.0035 ± 0.0004	0.8	3/9
	50–60%	–	0.088 ± 0.004	0.487 ± 0.011	3700 ± 158	0.0022 ± 0.0003	0.6	4/9
	60–70%	–	0.083 ± 0.006	0.480 ± 0.012	3530 ± 160	0.00175 ± 0.0004	0.3	4/9
	70–80%	–	0.081 ± 0.005	0.481 ± 0.009	3310 ± 130	0.00055 ± 0.00005	0.4	14/9
Figure 1 Au–Au 62.4 GeV	0–5%	Λ	0.137 ± 0.006	0.470 ± 0.009	4300 ± 152	0.023 ± 0.004	0.7	1/7
	5–10%	–	0.133 ± 0.005	0.468 ± 0.010	4120 ± 160	0.002 ± 0.0004	0.7	1/7
	10–20%	–	0.130 ± 0.006	0.470 ± 0.011	4000 ± 187	0.00017 ± 0.00004	0.7	1/7
	20–30%	–	0.126 ± 0.004	0.465 ± 0.010	3830 ± 164	$1 \times 10^{-5} \pm 4 \times 10^{-6}$	0.8	1/7
	30–40%	–	0.123 ± 0.004	0.467 ± 0.012	3650 ± 160	$9 \times 10^{-7} \pm 5 \times 10^{-8}$	0.8	1/7
	40–60%	–	0.120 ± 0.005	0.460 ± 0.011	3400 ± 156	$4 \times 10^{-8} \pm 3 \times 10^{-9}$	0.8	5/7
	60–80%	–	0.117 ± 0.005	0.460 ± 0.012	3200 ± 140	$1 \times 10^{-9} \pm 5 \times 10^{-10}$	0.9	5/7
Figure 1 Au–Au 62.4 GeV	0–5%	Ξ^+	0.138 ± 0.004	0.455 ± 0.011	4150 ± 150	0.0008 ± 0.00004	0.7	0.4/5
	5–10%	–	0.134 ± 0.005	0.450 ± 0.011	4000 ± 140	$6.5 \times 10^{-5} \pm 6 \times 10^{-6}$	1	3/6
	10–20%	–	0.131 ± 0.006	0.452 ± 0.012	3800 ± 157	$5.2 \times 10^{-6} \pm 4 \times 10^{-7}$	0.8	2/6
	20–40%	–	0.127 ± 0.004	0.450 ± 0.010	3600 ± 148	$4.5 \times 10^{-7} \pm 6 \times 10^{-8}$	0.7	3/6
	40–60%	–	0.124 ± 0.005	0.453 ± 0.010	3400 ± 150	$8.8 \times 10^{-9} \pm 5 \times 10^{-10}$	0.7	1/6
	60–80%	–	0.120 ± 0.005	0.450 ± 0.009	3200 ± 146	$3.4 \times 10^{-10} \pm 5 \times 10^{-11}$	0.4	3/4

Table 1. Cont.

Collisions	Centrality	Particle	T_0 (GeV)	β_T (c)	$V(fm^3)$	N_0	n_0	χ^2/dof
Figure 1 Au–Au 62.4 GeV	0–20%	$\bar{\Omega}^+$	0.138 ± 0.004	0.440 ± 0.008	4000 ± 155	$5.2 \times 10^{-5} \pm 5 \times 10^{-6}$	0.6	0.3/0
	20–40%	–	0.134 ± 0.006	0.435 ± 0.011	3800 ± 146	$2 \times 10^{-7} \pm 6 \times 10^{-8}$	1	1/0
	40–60%	–	0.127 ± 0.005	0.436 ± 0.012	3600 ± 160	$3.2 \times 10^{-9} \pm 7 \times 10^{-10}$	0.7	2/–1
Figure 1 Au–Au 62.4 GeV	0–10%	d	0.114 ± 0.005	0.400 ± 0.011	3400 ± 140	0.00085 ± 0.00005	1.6	3/7
	10–20%	–	0.109 ± 0.006	0.395 ± 0.010	3200 ± 150	0.00034 ± 0.00004	1.6	2/7
	20–40%	–	0.104 ± 0.005	0.396 ± 0.011	3000 ± 145	0.0001 ± 0.00004	1.5	1/7
	40–60%	–	0.097 ± 0.005	0.393 ± 0.012	2800 ± 170	$2 \times 10^{-5} \pm 5 \times 10^{-6}$	1.3	1/7
	60–80%	–	0.090 ± 0.004	0.392 ± 0.011	2632 ± 150	$2 \times 10^{-6} \pm 4 \times 10^{-7}$	0.9	22/6
Figure 2 Pb–Pb 2.76 TeV	0–5%	π^+	0.130 ± 0.005	0.584 ± 0.012	7000 ± 200	345 ± 36	0.8	89/36
	5–10%	–	0.127 ± 0.006	0.583 ± 0.010	6816 ± 191	165.55 ± 23	0.7	158/36
	10–20%	–	0.123 ± 0.004	0.580 ± 0.011	6650 ± 185	60.55 ± 8	0.8	93/36
	20–30%	–	0.119 ± 0.005	0.581 ± 0.010	6392 ± 180	18.80 ± 3	0.9	58/36
	30–40%	–	0.115 ± 0.005	0.580 ± 0.012	6200 ± 185	6.3 ± 0.4	1	54/36
	40–50%	–	0.112 ± 0.006	0.580 ± 0.011	6000 ± 170	2.2 ± 0.3	1	92/36
	50–60%	–	0.109 ± 0.004	0.581 ± 0.011	5843 ± 162	0.66 ± 0.04	1	100/36
	60–70%	–	0.106 ± 0.006	0.579 ± 0.010	5670 ± 170	0.16 ± 0.03	1.1	197/36
	70–80%	–	0.101 ± 0.005	0.578 ± 0.011	5500 ± 166	0.04 ± 0.005	1.1	151/36
80–90%	–	0.098 ± 0.004	0.576 ± 0.010	5300 ± 160	0.008 ± 0.0004	1.1	221/36	
Figure 2 Pb–Pb 2.76 TeV	0–5%	p	0.131 ± 0.005	0.570 ± 0.010	6700 ± 180	8 ± 0.7	1	58/30
	5–10%	–	0.127 ± 0.006	0.570 ± 0.010	6500 ± 170	4.05 ± 0.5	0.9	125/37
	10–20%	–	0.123 ± 0.005	0.570 ± 0.009	6320 ± 170	1.35 ± 0.3	1.1	37/33
	20–30%	–	0.120 ± 0.006	0.570 ± 0.011	6180 ± 160	0.9 ± 0.05	1.1	34/31
	30–40%	–	0.116 ± 0.005	0.565 ± 0.012	6000 ± 180	0.16 ± 0.04	1.07	17/31
	40–50%	–	0.112 ± 0.006	0.567 ± 0.009	5830 ± 170	0.05 ± 0.004	1.1	108/33
	50–60%	–	0.108 ± 0.005	0.564 ± 0.010	5650 ± 165	0.016 ± 0.003	1	62/31
	60–70%	–	0.104 ± 0.005	0.562 ± 0.011	5480 ± 170	0.0045 ± 0.0004	1	140/34
	70–80%	–	0.101 ± 0.005	0.562 ± 0.009	5300 ± 180	0.001 ± 0.0003	0.9	214/36
80–90%	–	0.097 ± 0.004	0.560 ± 0.010	5100 ± 180	0.0002 ± 0.00003	0.8	207/37	
Figure 2 Pb–Pb 2.76 TeV	0–10%	Λ	0.155 ± 0.005	0.500 ± 0.011	6000 ± 200	0.13 ± 0.03	0.9	28/14
	10–20%	–	0.152 ± 0.006	0.497 ± 0.009	5800 ± 180	0.1 ± 0.03	0.8	27/14
	20–40%	–	0.147 ± 0.004	0.496 ± 0.010	5600 ± 180	0.06 ± 0.004	0.8	35/14
	40–60%	–	0.142 ± 0.005	0.495 ± 0.011	5400 ± 185	0.024 ± 0.004	0.6	124/14
	60–80%	–	0.137 ± 0.005	0.494 ± 0.010	5200 ± 170	0.0074 ± 0.0005	1.1	17/14

Table 1. Cont.

Collisions	Centrality	Particle	T_0 (GeV)	β_T (c)	$V(fm^3)$	N_0	n_0	χ^2/dof
Figure 2 Pb–Pb 2.76 TeV	0–10%	Ξ	0.156 ± 0.006	0.480 ± 0.010	5500 ± 200	0.0180 ± 0.004	1	16/7
	10–20%	–	0.152 ± 0.005	0.477 ± 0.012	5300 ± 180	0.0140 ± 0.003	1	37/7
	20–40%	–	0.148 ± 0.005	0.474 ± 0.010	5126 ± 170	0.0085 ± 0.0005	0.9	63/7
	40–60%	–	0.144 ± 0.005	0.473 ± 0.009	4950 ± 160	0.0032 ± 0.0005	0.8	82/7
	60–80%	–	0.140 ± 0.006	0.470 ± 0.012	4700 ± 180	0.0008 ± 0.00005	0.6	107/7
Figure 2 Pb–Pb 2.76 TeV	0–10%	Ω	0.158 ± 0.005	0.460 ± 0.010	5000 ± 150	0.0014 ± 0.0003	1.1	12/2
	10–20%	–	0.154 ± 0.005	0.458 ± 0.009	4817 ± 160	$9.7 \times 10^{-4} \pm 4 \times 10^{-5}$	1.2	1/2
	20–40%	–	0.150 ± 0.004	0.457 ± 0.012	4600 ± 180	$6 \times 10^{-4} \pm 6 \times 10^{-5}$	0.9	3/2
	40–60%	–	0.147 ± 0.005	0.456 ± 0.010	4400 ± 120	$2 \times 10^{-4} \pm 5 \times 10^{-5}$	0.8	6/2
	60–80%	–	0.143 ± 0.004	0.453 ± 0.012	4200 ± 180	$4 \times 10^{-5} \pm 5 \times 10^{-6}$	0.7	5/1
Figure 2 Pb–Pb 2.76 TeV	0–10%	d	0.133 ± 0.005	0.430 ± 0.008	4500 ± 170	$4.6 \times 10^{-4} \pm 5 \times 10^{-5}$	1.8	6/16
	10–20%	–	0.130 ± 0.005	0.428 ± 0.011	4300 ± 160	$1.8 \times 10^{-4} \pm 4 \times 10^{-5}$	1.8	6/16
	20–40%	–	0.126 ± 0.006	0.426 ± 0.009	4100 ± 153	$6.6 \times 10^{-5} \pm 4 \times 10^{-6}$	1.7	4/16
	40–60%	–	0.122 ± 0.004	0.423 ± 0.011	3938 ± 160	$1.5 \times 10^{-5} \pm 5 \times 10^{-6}$	1.2	15/10
	60–80%	–	0.118 ± 0.005	0.422 ± 0.012	3650 ± 150	$2.8 \times 10^{-6} \pm 4 \times 10^{-7}$	1.3	10/10

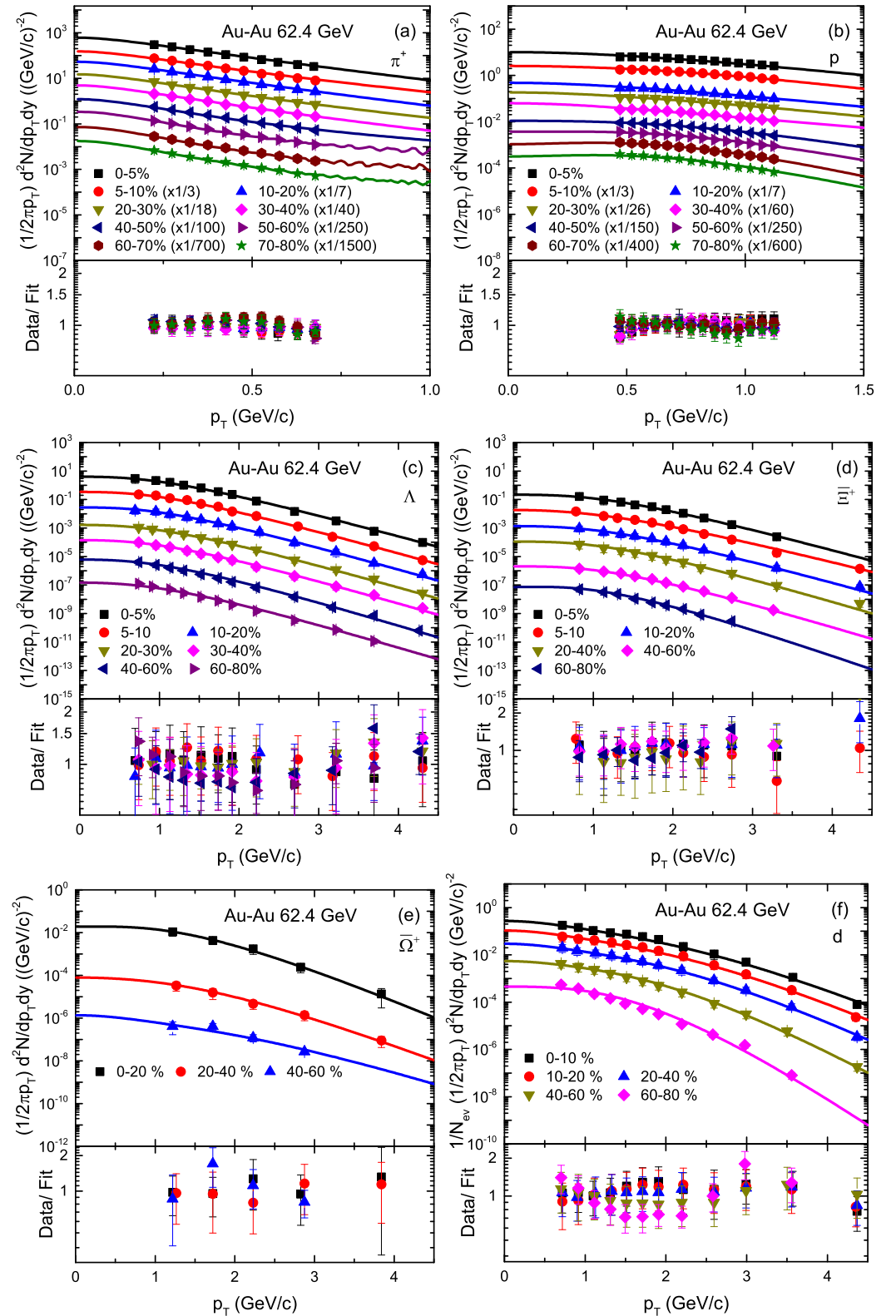


Figure 1. Transverse momentum spectra of π^+ , p , Λ , Ξ and Ω rapidity at $|y| < 0.1$, and deuteron (d) at rapidity $|y| < 0.3$, produced in different centrality intervals in Au–Au collisions at 62.4 GeV. Different symbols represent the p_T spectra of different particles measured by the STAR collaboration [21,55,56] and the curves are our fitted results with the blast wave model with Boltzmann Gibbs statistics (BGBW). The corresponding results of the data/fit are presented in each panel.

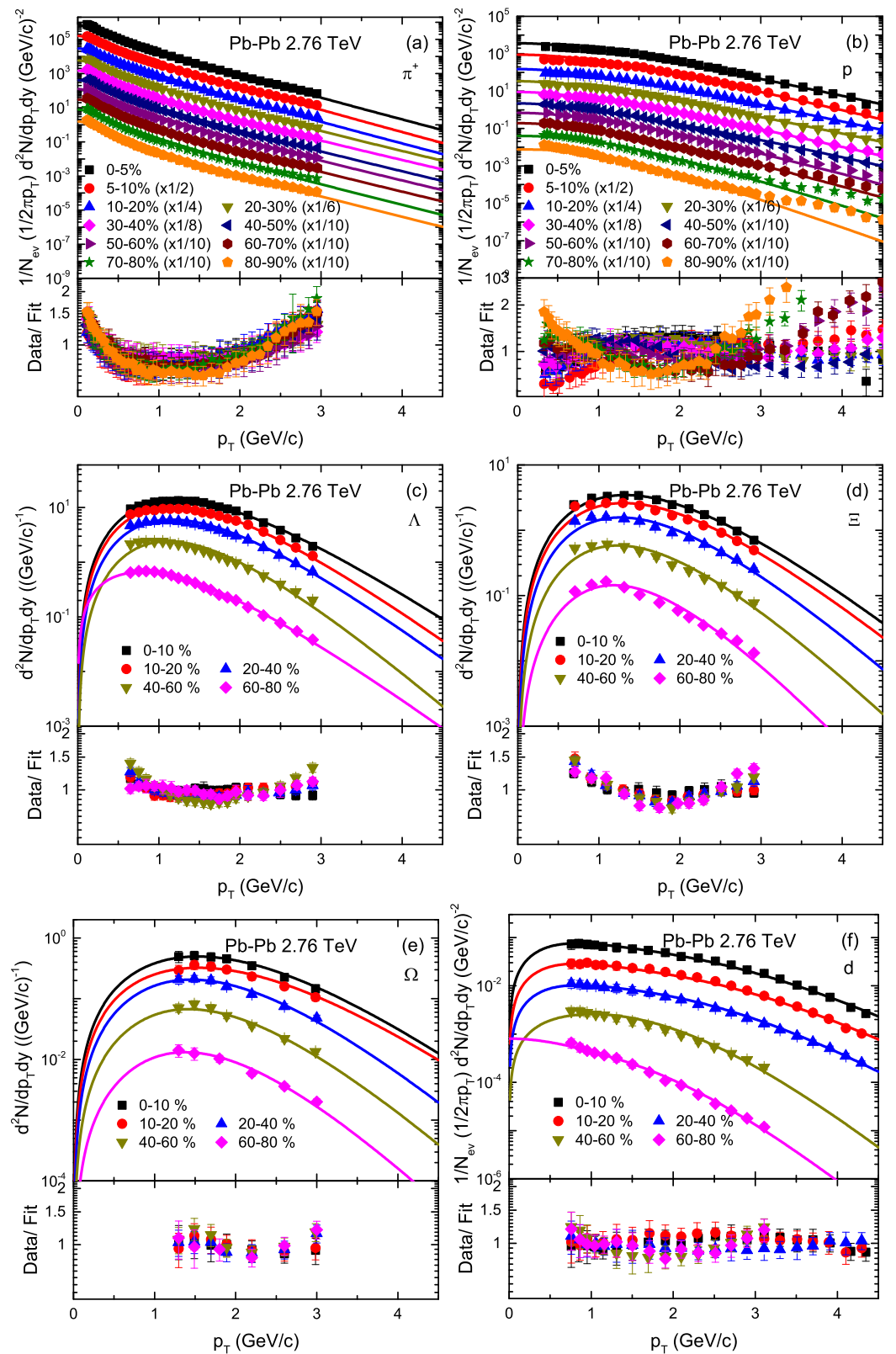


Figure 2. Transverse momentum spectra of π^+ , p , Λ , Ξ , Ω and deuteron (d) produced in different centrality intervals in Pb–Pb collisions at 2.76 TeV at rapidity $|y| < 0.5$. Different symbols represent the p_T spectra of different particles measured by the ALICE collaboration [57–59] and the curves are our fitted results with the BGBW model. The corresponding results of the data/fit are presented in each panel.

Figure 3 shows the dependence of the kinetic freezeout temperature (T_0) on the centrality class ($C\%$) and mass of the particles. Panels (a) and (b) show the results for Au–Au and Pb–Pb collisions, respectively. The colored symbols represent different species of particles, and the particles from left to right show the result of T_0 from central to peripheral collisions. One can see that the kinetic freezeout temperature of the emission source decreases with the decrease of centrality from central to peripheral collisions. The central collision corresponds to a very violent collision due to the large number of participant nucleons, which makes the degree of excitation of the system high and results in a high temperature, but as the centrality decreases, the collision becomes decreasingly violent due to the small number of particles involved in the interaction, which results in the degree of excitation of the system decreasing, and correspondingly the temperature decreases. This result is consistent with [5,6,18,27–29,60], but inconsistent with [61–65]. In addition, the dependence of T_0 on m_0 is not clear. The pion and proton have almost the same values for T_0 , and similarly the strange (multi-strange) particles have almost the same values for T_0 . Deuteron has the largest mass, and it freezes out at the same time as the pion and proton. The reason may be the production cross-section of the interacting particle. According to kinematics, the reactions with a smaller cross-section are supposed to be switched-off at higher temperatures/densities or earlier in time than the reactions with larger cross-sections. π^+ , p and d are non-strange particles, so they have the same T_0 , while Λ , $\Xi(\Xi^+)$ and $\Omega(\bar{\Omega}^+)$ are strange-flavored particles, so they have the same T_0 . The non-strange particles have a larger production cross-section than the strange or multi-strange particles; therefore, the non-strange particles freezeout later than the strange (multi-strange) particles. This result is consistent with that of our recent work [10]; however, in [10], the authors also observed a separate decoupling of strange and multi-strange particles. It is noteworthy that the observed T_0 at the RHIC is lower than that of the LHC. In addition, we would also like to point out that several previous works have studied the fit of the blast wave with different methods and obtained different results from those of our recent work. In the present work, the least square method is used, and we observed the double kinetic freezeout scenario, while the previous literature observed single or multiple kinetic freezeout scenarios.

Figure 4 is similar to Figure 3, but shows the dependence of the transverse flow velocity (β_T) on the centrality class and mass of the particles. One can see that β_T depends on the resting mass of the particles. The greater the mass of the particle, the smaller the transverse flow velocity. In fact, some hydrodynamic simulations observed the same velocity for the flow of all the particles, but they presented different explanations. Besides, different models give different results. The selection of β_T is more technical and complex; in some cases, it even depends on the range of p_T , such that the selections of ranges are different for different models. Furthermore, there is no centrality dependence of β_T observed in the present work, as β_T is almost the same in the central and peripheral collisions. The reason behind this is that the collective behavior at the stage of kinetic freezeout does not change from central to peripheral collisions. However, β_T is larger at the LHC than that of the RHIC.

Figure 5 is similar to Figures 3 and 4 but shows the dependence of V on the centrality class and mass of the particles. One can see that V decreases continuously from central to peripheral collisions because the central collisions correspond to a large number of binary collisions due to the re-scattering of partons, and hence the system with more participants quickly reaches the equilibrium state, while the number of participants decreases with the decrease of event centrality and the system reaches an equilibrium state in a steady manner from central to peripheral collisions. Additionally, V depends on the mass of the particles. The greater the mass of the particle, the lower the V . V at the LHC is larger than that at the RHIC.

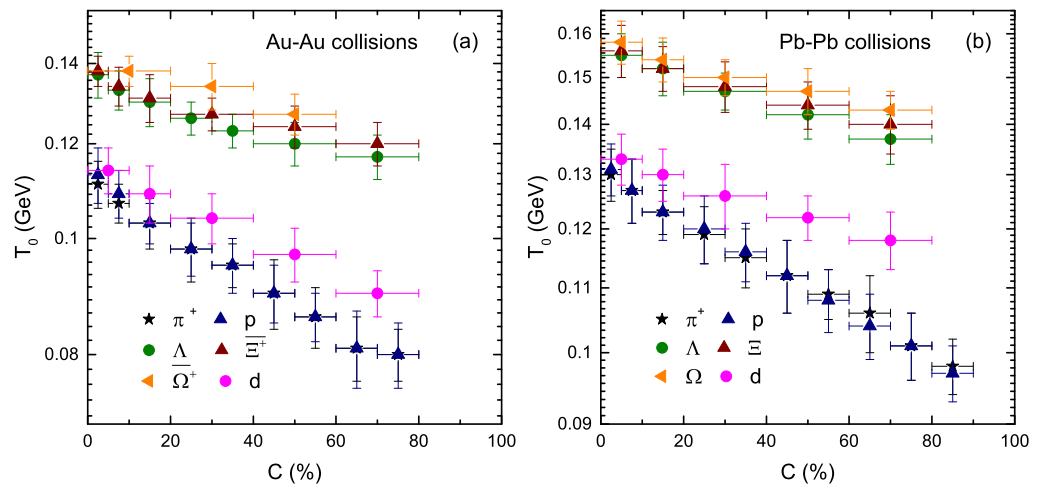


Figure 3. Dependence of T_0 on the centrality class ($C\%$) and resting mass (m_0) of the particle.

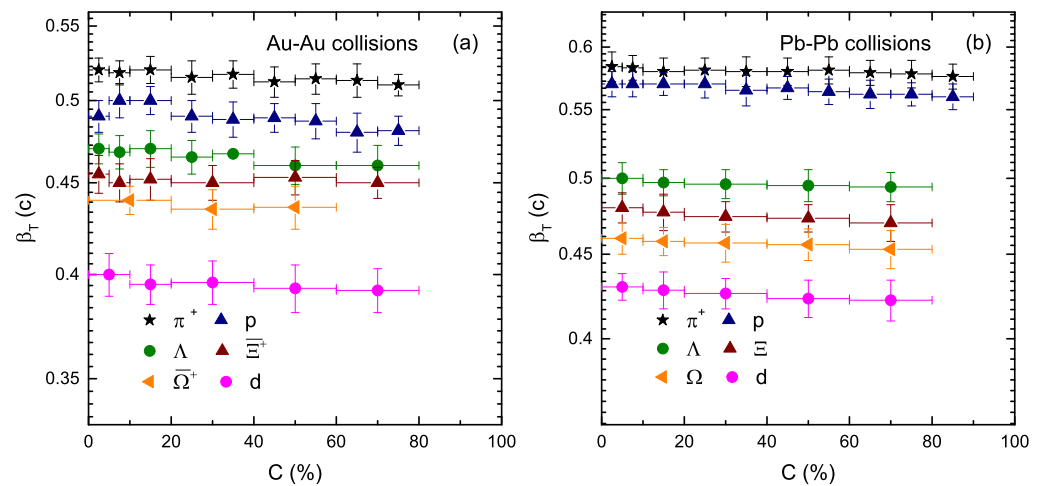


Figure 4. Dependence of β_T on the centrality class ($C\%$) and resting mass (m_0) of the particle.

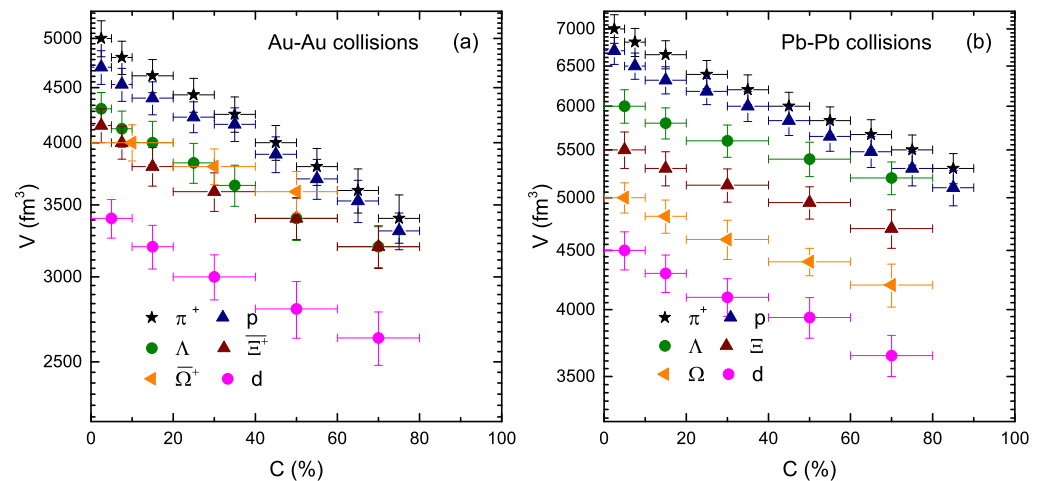


Figure 5. Dependence of V on the centrality class ($C\%$) and resting mass (m_0) of the particle.

It should be noted that the cases of T_0 and/or β_T are very complex on the basis of their dependence on centrality. The observed results can be changed by changing the model, by using the same model but a different method or by changing the limits and conditions of the model, such that by changing the parameters, we can get different results. For example, if for central collisions, one use a smaller T_0 and a larger β_T , a decreasing trend for T_0 from peripheral to central collisions can be obtained. At the same time, a negative correlation

between T_0 and β_T will also be obtained. Similarly, if one use a larger T_0 and a smaller β_T , an increasing trend for T_0 from peripheral to central collisions can be obtained. At the same time, a positive correlation between T_0 and β_T will also be obtained.

4. Conclusions

The main observations and conclusions of our work are summarized here.

- (a) The transverse momentum spectra of different particle species are analyzed by the blast wave model with Boltzmann Gibbs statistics, and the bulk properties in terms of the kinetic freezeout temperature, transverse flow velocity and freezeout volume are extracted in different centrality classes in nucleus–nucleus collisions at center of mass energy.
- (b) It is observed that T_0 is dependent on the cross-section of the interacting particle; i.e., a larger production cross-section of the interacting particle corresponds to a smaller T_0 .
- (c) A double kinetic freezeout scenario is observed due to the separate decoupling of non-strange and strange (multi-strange) particles.
- (d) The transverse flow velocity (β_T) and kinetic freezeout volume (V) are observed to depend on the mass of the particles; i.e., the larger the mass of the particle, the smaller the β_T and V .
- (e) The kinetic freezeout temperature (T_0) and freezeout volume (V) decrease from central peripheral collisions due to the decrease of the degree of excitation of the interacting system and the decrease of the number of binary collisions due to the re-scattering of partons from central to peripheral collisions, respectively. At the same time, β_T is observed to be independent of centrality and remains almost unchanged from central to peripheral collisions because the collective behavior at the stage of the kinetic freezeout in the interacting system does not change with event centrality.
- (f) T_0 , β_T and V are observed to be larger for collisions at the LHC than at the RHIC.
- (g) The obtained results can be changed by changing the model, by using the same model with a different method or by changing the parameters used in the model.

Author Contributions: Conceptualization, M.W.; Methodology, M.W. and G.-X.P.; Software, M.W.; Validation, M.W. and G.-X.P.; Formal analysis, M.W.; Investigation, M.W.; Resources, G.-X.P.; Data curation, M.W.; Writing—original draft preparation, M.W.; writing—review and editing, M.W.; visualization, M.W.; supervision, G.-X.P.; project administration, G.-X.P.; funding acquisition, G.-X.P. All authors have read and agreed to the published version of the manuscript.

Funding: This work was supported by the National Natural Science Foundation of China under Grant Nos. 11875052, 11575190, and 11135011.

Institutional Review Board Statement: The authors declare that they are in compliance with ethical standards regarding the content of this paper.

Informed Consent Statement: Not applicable.

Data Availability Statement: The data used to support the findings of this study are included within the article and are cited at relevant places within the text as references.

Acknowledgments: The authors would like to express thanks for support from the National Natural Science Foundation of China (Grant Nos. 11875052, 11575190, and 11135011).

Conflicts of Interest: The authors declare that there are no conflicts of interest regarding the publication of the paper. The funding agencies have no role in the design of the study; in the collection, analysis, or interpretation of the data; in writing the manuscript, or in the decision to publish the results.

References

1. Cleymans, J.; Oeschler, H.; Redlich, K.; Wheaton, S. Comparison of chemical freeze-out criteria in heavy-ion collisions. *Phys. Rev. C* **2006**, *73*, 034905. [[CrossRef](#)]
2. Andronic, A.; Braun-Munzinger, P.; Stachel, J. Hadron production in central nucleus-nucleus collisions at chemical freeze-out. *Nuclear Phys. A* **2006**, *772*, 167–199. [[CrossRef](#)]
3. Andronic, A.; Braun-Munzinger, P.; Stachel, J. The Horn, the hadron mass spectrum and the QCD phase diagram: The Statistical model of hadron production in central nucleus-nucleus collisions. *Nuclear Phys. A* **2010**, *834*, 237C–240C. [[CrossRef](#)]
4. Andronic, A.; Braun-Munzinger, P.; Stachel, J. Thermal hadron production in relativistic nuclear collisions. *Acta Phys. Pol. B* **2009**, *40*, 1005–1012.
5. Waqas, M.; Liu, F.-H.; Fakhraddin, S.; Rahim, M.A. Possible scenarios for single, double, or multiple kinetic freeze-out in high energy collisions. *Indian J. Phys.* **2019**, *93*, 1329–1343. [[CrossRef](#)]
6. Waqas, M.; Li, B.C. Kinetic freeze-out temperature and transverse flow velocity in Au-Au collisions at RHIC-BES energies. *Adv. High Energy Phys.* **2020**, *2020*, 1787183. [[CrossRef](#)]
7. Khuntia, A.; Sharma, H.; Tiwari, S.K.; Sahoo, R.; Cleymans, J. Radial flow and differential freeze-out in proton-proton collisions at $\sqrt{s} = 7$ TeV at the LHC. *Eur. Phys. J. A* **2019**, *55*, 3. [[CrossRef](#)]
8. Thakur, D.; Tripathy, S.; Garg, P.; Sahoo, R.; Cleymans, J. Indication of differential kinetic freeze-out at RHIC and LHC energies. *Acta Phys. Pol. Supp.* **2016**, *9*, 329. [[CrossRef](#)]
9. Shao, M.; Yi, L.; Tang, Z.; Chen, H.; Li, C.; Xu, Z. Examination of the species and beam energy dependence of particle spectra using Tsallis statistics. *J. Phys. G* **2010**, *37*, 085104. [[CrossRef](#)]
10. Waqas, M.; Peng, G.X.; Liu, F.-H. *An Evidence of Triple Kinetic Freezeout Scenario Observed in All Centrality Intervals in Cu-Cu, Au-Au and Pb-Pb Collisions at High Energies*; IOP Publishing Ltd.: Bristol, UK, 2020.
11. Abelev, B.; Adam, J.; Adamova, D.; Adare, A.M.; Aggarwal, M.M.; Rinella, G.A.; Agocs, A.G.; Agostinelli, A.; Salazar, S.A.; Ahammed, Z.; et al. Pion, Kaon, and Proton Production in Central Pb–Pb Collisions at $\sqrt{s_{NN}} = 2.76$ TeV. *Phys. Rev. Lett.* **2012**, *109*, 252301. [[CrossRef](#)]
12. Andronic, A. An overview of the experimental study of quark-gluon matter in high-energy nucleus-nucleus collisions. *Int. J. Mod. Phys. A* **2014**, *29*, 1430047. [[CrossRef](#)]
13. Zhang, S.; Ma, Y.G.; Chen, J.H.; Zhong, C. Production of Kaon and Λ in Nucleus-Nucleus Collisions at Ultrarelativistic Energy from a Blast-Wave Model. *Adv. High Energy Phys.* **2015**, *2015*, 460590. [[CrossRef](#)]
14. Zhang, S.; Ma, Y.G.; Chen, J.H.; Zhong, C. Beam energy dependence of Hanbury-Brown-Twiss radii from a blast-wave model. *Adv. High Energy Phys.* **2016**, *2016*, 9414239. [[CrossRef](#)]
15. Waqas, M.; Liu, F.-H.; Li, L.L.; Alfanda, H.M. Effective (kinetic freeze-out) temperature, transverse flow velocity and kinetic freeze-out volume in high energy collisions. *Nuclear Sci. Tech.* **2010**, *31*, 109. [[CrossRef](#)]
16. Waqas, M.; Liu, F.-H.; Wazir, Z. Dependence of temperatures and kinetic freeze-out volume on centrality in Au-Au and Pb-Pb collisions at high energy. *Adv. High Energy Phys.* **2020**, *2020*, 8198126. [[CrossRef](#)]
17. Waqas, M.; Liu, F.-H. *Centrality Dependence of Kinetic Freeze-Out Temperature and Transverse Flow Velocity in High Energy Nuclear Collisions*; Springer: Berlin/Heidelberg, Germany, 2021.
18. Wang, Q.; Liu, F.-H. Initial and final state temperatures of antiproton emission sources in high energy collisions. *Int. J. Theor. Phys.* **2019**, *58*, 4119–4138. [[CrossRef](#)]
19. Schnedermann, E.; Sollfrank, J.; Heinz, U.W. Thermal phenomenology of hadrons from 200-A/GeV S+S collisions. *Phys. Rev. C* **1993**, *48*, 2462–2475. [[CrossRef](#)]
20. Abelev, B.I.; Aggarwal, M.M.; Ahammed, Z.; Alakhverdyants, A.V.; Anderson, B.D.; Arkhipkin, D.; Averichev, G.S.; Balewski, J.; Barannikova, O.; Barnby, L.S.; et al. Identified particle production, azimuthal anisotropy, and interferometry measurements in Au+Au collisions at $s(NN)^{1/2} = 9.2$ -GeV. *Phys. Rev. C* **2010**, *81*, 024911. [[CrossRef](#)]
21. Abelev, B.I.; Aggarwal, M.M.; Ahammed, Z.; Anderson, B.D.; Arkhipkin, D.; Averichev, G.S.; Bai, Y.; Balewski, J.; Barannikova, O.; Barnby, L.S.; et al. Systematic Measurements of Identified Particle Spectra in pp, d^+ Au and Au+Au Collisions from STAR. *Phys. Rev. C* **2009**, *79*, 034909. [[CrossRef](#)]
22. Tang, Z.; Yi, L.; Ruan, L.; Shao, M.; Chen, H.; Li, C.; Mohanty, B.; Sorensen, P.; Tang, A.; Xu, Z. The statistical origin of constituent-quark scaling in QGP hadronization. *Chin. Phys. Lett.* **2013**, *30*, 031201. [[CrossRef](#)]
23. Jiang, K.; Zhu, Y.; Liu, W.; Chen, H.; Li, C.; Ruan, L.; Tang, Z.; Xu, Z. Onset of radial flow in p+ p collisions. *Phys. Rev. C* **2015**, *91*, 024910. [[CrossRef](#)]
24. Tang, Z.; Xu, Y.; Ruan, L.; van Buren, G.; Wang, F.; Xu, Z. Spectra and radial flow in relativistic heavy ion collisions with Tsallis statistics in a blast-wave description. *Phys. Rev. C* **2009**, *79*, 051901. [[CrossRef](#)]
25. Wei, H.R.; Liu, F.-H.; Lacey, R.A. Kinetic freeze-out temperature and flow velocity extracted from transverse momentum spectra of final-state light flavor particles produced in collisions at RHIC and LHC. *Eur. Phys. J. A* **2016**, *52*, 102. [[CrossRef](#)]
26. Wei, H.R.; Liu, F.-H.; Lacey, R.A. Disentangling random thermal motion of particles and collective expansion of source from transverse momentum spectra in high energy collisions. *J. Phys. G* **2016**, *43*, 125102. [[CrossRef](#)]
27. Lao, H.-L.; Wei, H.R.; Liu, F.-H.; Lacey, R.A. An evidence of mass-dependent differential kinetic freeze-out scenario observed in Pb-Pb collisions at 2.76 TeV. *Eur. Phys. J. A* **2016**, *52*, 203. [[CrossRef](#)]

28. Lao, H.-L.; Liu, F.-H.; Li, B.C.; Duan, M.Y.; Lacey, R.A. Examining the model dependence of the determination of kinetic freeze-out temperature and transverse flow velocity in small collision system. *Nuclear Sci. Tech.* **2018**, *29*, 164. [[CrossRef](#)]
29. Lao, H.-L.; Liu, F.-H.; Li, B.C.; Duan, M.Y. Kinetic freeze-out temperatures in central and peripheral collisions: Which one is larger? *Nuclear Sci. Tech.* **2018**, *29*, 82. [[CrossRef](#)]
30. Zheng, H.; Zhu, L. Comparing the Tsallis distribution with and without thermodynamical description in $p + p$ collisions. *Adv. High Energy Phys.* **2016**, *2016*, 9632126. [[CrossRef](#)]
31. Cleymans, J.; Worku, D. Relativistic Thermodynamics: Transverse Momentum Distributions in High-Energy Physics. *Eur. Phys. J. A* **2012**, *48*, 160. [[CrossRef](#)]
32. Takeuchi, S.; Murase, K.; Hirano, T.; Huovinen, P.; Nara, Y. Effects of hadronic rescattering on multistrange hadrons in high-energy nuclear collisions. *Phys. Rev. C* **2015**, *92*, 044907. [[CrossRef](#)]
33. Heinz, U.W. Hydrodynamics at RHIC: How well does it work, where and how does it break down? *J. Phys. Nuclear Part. Phys.* **2005**, *31*, S717. [[CrossRef](#)]
34. Heiselberg, H.; Levy, A.-M. Elliptic flow and HanburyBrown CTwiss correlations in noncentral nuclear collisions. *Phys. Rev. C* **1999**, *59*, C2716–C2727. [[CrossRef](#)]
35. Russo, R. Measurement of D^+ meson production in p-Pb collisions with the ALICE detector. *arXiv* **2015**, arXiv:1511.04380.
36. Biró, G.; Barnaföldi, G.G.; Biró, T.S.; Ürmössy, K.; Takács, Á. Systematic analysis of the non-extensive statistical approach in high energy particle collisions—experiment vs. theory. *Entropy* **2017**, *19*, 88. [[CrossRef](#)]
37. Sadhu, S.; Ghosh, P. Anomalous features of particle production in high-multiplicity events of p p collisions at the LHC energies. *Phys. Rev. D* **2019**, *99*, 034020. [[CrossRef](#)]
38. Chatrchyan, S.; Apresyan, A.; Bornheim, A.; Bunn, J. Study of high-pT charged particle suppression in PbPb compared to pp collisions at $\sqrt{s_{NN}} = 2.76$ TeV. *Eur. Phys. J. C* **2012**, *72*, 1945. [[CrossRef](#)]
39. Tsallis, C. Possible Generalization of Boltzmann-Gibbs Statistics. *J. Stat. Phys.* **1988**, *52*, 479–487. [[CrossRef](#)]
40. Abelev, B.I.; Adams, J.; Aggarwal, M.M.; Ahammed, Z.; Amonett, J.; Anderson, B.D.; Anderson, M.; Arkhipkin, D.; Averichev, G.S.; Bai, Y.; et al. Strange particle production in p + p collisions at 200 GeV. *Phys. Rev.* **2007**, *75*, 064901.
41. Petrovici, M.; Andrei, C.; Berceau, I.; Bercuci, A.; Herghelegiu, A.; Pop, A. Recent results and open questions on collective type phenomena from AA to pp collisions. *AIP Conf. Proc.* **2015**, *1645*, 52–60. [[CrossRef](#)]
42. Hagedorn, R. Multiplicities, p_T distributions and the expected hadron quark-gluon phase transition. *Riv. Del Nuovo C.* **1983**, *6*, 1–50. [[CrossRef](#)]
43. Suleymanov, M. The meaning behind observed p T regions at the LHC energies. *Int. J. Mod. Phys. E* **2018**, *27*, 1850008. [[CrossRef](#)]
44. Khachatryan, V.; Sirunyan, A.M.; Tumasyan, A.; Adam, W.; Bergauer, T.; Dragicevic, M.; Erö, J.; Friedl, M.; Fruehwirth, R.; Ghete, V.M.; et al. Production of $\Sigma(1385)^\pm$ and $\Xi(1530)^0$ in proton-proton collisions at $\sqrt{s} = 7$ TeV. *Eur. Phys. J. C* **2015**, *75*. [[CrossRef](#)]
45. Odorico, R. Does a transverse energy trigger actually trigger on large-PT jets? *Phys. Lett. B* **1982**, *118*, 151–154. [[CrossRef](#)]
46. Arnison, G.; Astbury, A.; Aubert, B.; Bacci, C.; Bernabei, R.; Bezaguet, A.; Böck, R.; Bowcock, T.J.; Calvetti, M.; Carroll, T.; et al. Transverse momentum spectra for charged particles at the CERN protonantiproton collider. *Phys. Lett. B* **1982**, *118*, 167–172. [[CrossRef](#)]
47. Biyajima, M.; Mizoguchi, T.; Suzuki, N. Analyses of whole transverse momentum distributions in $p\bar{p}$ and pp collisions by using a modified version of Hagedorn's formula. *Int. J. Mod. Phys. A* **2017**, *32*, 1750057. [[CrossRef](#)]
48. Aamodt, K.; Abelev, B.; Quintana, A.A.; Adamova, D.; Adare, A.M.; Aggarwal, M.M.; Rinella, G.A.; Agocs, A.G.; Agostinelli, A.; Salazar, S.A.; et al. Heavy flavour decay muon production at forward rapidity in proton-proton collisions at $\sqrt{s} = 7$ TeV. *Phys. Lett. B* **2012**, *708*, 265–275. [[CrossRef](#)]
49. Lakomov, I. Event activity dependence of inclusive J/ψ production in p-Pb collisions at $\sqrt{s_{NN}} = 5.02$ TeV with ALICE at the LHC. *Nuclear Phys. A* **2014**, *931*, 1179–1183. [[CrossRef](#)]
50. Abelev, B.; Adam, J.; Adamová, D.; Adare, A.M.; Aggarwal, M.M.; Rinella, G.A.; Agocs, A.G.; Agostinelli, A.; Salazar, S.A.; Ahammed, Z.; et al. Inclusive J/ψ production in pp collisions at $\sqrt{s} = 2.76$ TeV. *Phys. Lett. B* **2012**, *718*, 295–306; Erratum in *Phys. Lett. B* **2015**, *748*, 472–473. [[CrossRef](#)]
51. Abelev, B.; Quintana, A.A.; Adamová, D.; Adare, A.M.; Aggarwal, M.M.; Rinella, G.A.; Agocs, A.G.; Agostinelli, A.; Salazar, S.A.; Ahammed, Z.; et al. Light vector meson production in pp collisions at $\sqrt{s} = 7$ TeV. *Phys. Lett. B* **2012**, *710*, 557–568. [[CrossRef](#)]
52. Abt, I.; Adams, M.; Agari, M.; Albrecht, H.; Aleksandrov, A.; Amaral, V.; Amorim, A.; Aplin, S.J.; Aushev, V.; Bagaturia, Y.; et al. $K^*(0)$ and phi meson production in proton-nucleus interactions at root $\sqrt{s} = 41.6$ GeV. *Eur. Phys. J. C* **2007**, *50*, 315–328. [[CrossRef](#)]
53. De Falco, A. Vector meson production in pp collisions at $\sqrt{s} = 7$ TeV, measured with the ALICE detector. *J. Phys. G* **2011**, *38*, 124083. [[CrossRef](#)]
54. Aamodt, K.; Abel, N.; Abeysekara, U.; Quintana, A.A.; Abramyan, A.; Adamová, D.; Aggarwal, M.M.; Rinella, G.A.; Agocs, A.G.; Salazar, S.A.; et al. Transverse momentum spectra of charged particles in proton-proton collisions at $\sqrt{s} = 900$ GeV with ALICE at the LHC. *Phys. Lett. B* **2010**, *693*, 53–68. [[CrossRef](#)]
55. Aggarwal, M.M.; Ahammed, Z.; Alakhverdyants, A.V.; Alekseev, I.; Alford, J.; Anderson, B.D.; Anson, C.D.; Arkhipkin, D.; Averichev, G.S.; Balewski, J.; et al. Strange and multistrange particle production in Au+ Au collisions at $\sqrt{s_{NN}} = 62.4$ GeV. *Phys. Rev. C* **2011**, *83*, 024901. [[CrossRef](#)]

56. Adam, J.; Adamczyk, L.; Adams, J.R.; Adkins, J.K.; Agakishiev, G.; Aggarwal, M.M.; Ahammed, Z.; Alekseev, I.; Anderson, D.M.; Aoyama, R.; et al. Beam energy dependence of (anti-) deuteron production in Au+ Au collisions at the BNL Relativistic Heavy Ion Collider. *Phys. Rev. C* **2019**, *99*, 064905. [[CrossRef](#)]
57. Abelev, B.; Adam, J.; Adamová, D.; Adare, A.M.; Aggarwal, M.M.; Rinella, G.A.; Agnello, M.; Agocs, A.G.; Agostinelli, A.; Ahammed, Z.; et al. Centrality dependence of π , K, and p production in Pb-Pb collisions at $\sqrt{s_{NN}} = 2.76$ TeV. *Phys. Rev. C* **2013**, *88*, 044910. [[CrossRef](#)]
58. Begun, V.; Florkowski, W.; Rybczynski, M. Transverse-momentum spectra of strange particles produced in Pb+ Pb collisions at $\sqrt{s_{NN}} = 2.76$ TeV in the chemical nonequilibrium model. *Phys. Rev. C* **2014**, *90*, 054912. [[CrossRef](#)]
59. Adam, J.; Adamová, D.; Aggarwal, M.M.; Rinella, G.A.; Agnello, M.; Agrawal, N.; Ahammed, Z.; Ahmed, I.; Ahn, S.U.; Aimo, I.; et al. Production of light nuclei and anti-nuclei in pp and Pb-Pb collisions at energies available at the CERN Large Hadron Collider. *Phys. Rev. C* **2016**, *93*, 024917. [[CrossRef](#)]
60. Waqas, M.; Liu, F.-H. Initial, effective, and kinetic freeze-out temperatures from transverse momentum spectra in high-energy proton (deuteron)–nucleus and nucleus–nucleus collisions. *Eur. Phys. J. Plus* **2020**, *135*, 147. [[CrossRef](#)]
61. Che, G.R.; Gu, J.B.; Zhang, W.C.; Zheng, H. Identified particle spectra in Pb-Pb and p-Pb collisions with a modified Tsallis blast-wave model. *arXiv* **2020**, arXiv:2010.14880.
62. Bashir, I.; Uddin, S. Centrality Dependence of $K^*(892)^0$ and $\phi(1020)$ Production at LHC. *Commun. Theor. Phys.* **2017**, *68*, 500. [[CrossRef](#)]
63. Uddin, S.; Bhat, R.A.; Bashir, I.U. Study of Centrality Dependence of Transverse Momentum Spectra of Hadrons and the Freeze-out Parameters at root (sNN) of 62.4 GeV, 130 GeV and 200 GeV. *arXiv* **2014**, arXiv:1412.2663.
64. Waqas, M.; Peng, G.X. Study of Proton, Deuteron, and Triton at 54.4 GeV. *Adv. High Energy Phys.* **2021**. Available online: <https://www.hindawi.com/journals/ahep/2021/6674470/> (accessed on 14 April 2021).
65. Acharya, S.; Adamova, D.; Adhya, S.P.; Adler, A.; Adolfsson, J.; Aggarwal, M.M.; Rinella, G.A.; Agnello, M.; Agrawal, N.; Ahammed, Z.; et al. Production of charged pions, kaons, and (anti-) protons in Pb-Pb and inelastic p p collisions at $\sqrt{s_{NN}} = 5.02$ TeV. *Phys. Rev. C* **2020**, *101*, 044907. [[CrossRef](#)]